Geophys. J. Int. (2009) **176,** 542–554 doi: 10.1111/j.1365-246X.2008.03985.x

Consistent phase picking for regional tomography models: application to the greater Alpine region

T. Diehl,[1]* E. Kissling,[1] S. Husen[2] and F. Aldersons[3]

[1]*Institute of Geophysics, Swiss Federal Institute of Technology, ETH Hönggerberg,* CH-8093 *Zürich, Switzerland*
[2]*Swiss Seismological Service, Swiss Federal Institute of Technology, ETH Hönggerberg,* CH-8093 *Zürich, Switzerland*
[3]*Scientific Consulting, Mies, Switzerland. http://faldersons.net*

Accepted 2008 September 17. Received 2008 September 17; in original form 2008 April 15

SUMMARY

The resolution and reliability of tomographic velocity models strongly depends on quality and consistency of available traveltime data. Arrival times routinely picked by network analysts on a day-to-day basis often yield a high level of noise due to mispicks and other inconsistencies, particularly in error assessment. Furthermore, tomographic studies at regional scales require merging of phase picks from several networks. Since a common quality assessment is not usually available for phase data provided by different networks, additional inconsistencies are introduced by the merging process. Considerable improvement in the quality of phase data can only be achieved through complete repicking of seismograms. Considering the amount of data necessary for regional high-resolution tomography, algorithms combining accurate picking with an automated error assessment represent the best tool to derive large suitable data sets. In this work, we present procedures for consistent automated and routine picking of *P*-wave arrival times at local to regional scales including consistent picking error assessment. Quality-attributed automatic picks are derived from the MPX picking system. The application to earthquakes in the greater Alpine region demonstrates the potential of such a repicking approach. The final data set consists of more than 13 000 high-quality first-arrivals and it is used to derive regional 1-D and preliminary 3-D *P*-wave models of the greater Alpine region. The comparison with a tomographic model based on routine phase data extracted from the ISC Bulletin illustrates effects on tomographic results due to consistency and reliability of our high-quality data set.

Key words: Tomography; Body waves; Crustal structure.

1 INTRODUCTION

Due to increasing computational power and major improvements in forward and inverse algorithms over the past two decades, seismic tomography is by now able to provide 3-D velocity images with spatial resolution of up to a few kilometres at local to regional scales. The development of sophisticated forward solution methods (e.g. ray tracing) for complex 3-D media (e.g. Um & Thurber 1987; Virieux *et al.* 1988; Podvin & Lecomte 1991) and their implementation in local earthquake tomography algorithms (e.g. Thurber 1983; Haslinger & Kissling 2001; Husen & Kissling 2001) have led to a significant increase in the computational accuracy of inversion techniques. The enlarged memory capacity of modern computer systems allows a fine grid for the model parametrization as described, for example, in Kissling *et al.* (2001).

The minimum resolvable velocity perturbation in tomographic models, however, depends directly on the model parametrization, the background velocity, and the timing accuracy of forward solvers and data. To resolve a velocity perturbation of $\Delta v = 5$ per cent in the mid-crust ($v_P \approx 6.0$ km s^{-1}) along a ray segment of $\Delta x =$ 15 km requires a timing error ε_t not greater than 0.12 s. The same perturbation amplitude along the same ray segment in the uppermost mantle ($v_P \approx 8.0$ km s^{-1}) requires an even higher timing accuracy of $\varepsilon_t < 0.09$ s.

Although modern forward solvers for complex 3-D structure are able to achieve such precision, the limiting factor of most present day tomographic studies is represented by the accuracy and consistency of the available phase data (i.e. phase picks). In this context, a 'phase pick' is defined as the arrival time of a seismic phase as determined from picking the onset of a wave at a particular station. Furthermore, we define 'routine pick' as the arrival time estimated by network analysts on a day-to-day basis for the purpose of locating earthquakes in near real-time. Differences in the picking behaviour of the various analysts of a network leads to inconsistencies in routine phase picks in terms of absolute timing (e.g. Leonard 2000), timing uncertainties and phase interpretations.

Additional inconsistencies across networks have to be considered for tomographic studies at regional scales. A uniform resolution of

*Now at: Lamont-Doherty Earth Observatory, Columbia University, Palisades, New York, USA. E-mail: tdiehl@ldeo.columbia.edu

© 2008 The Authors
Journal compilation © 2008 RAS

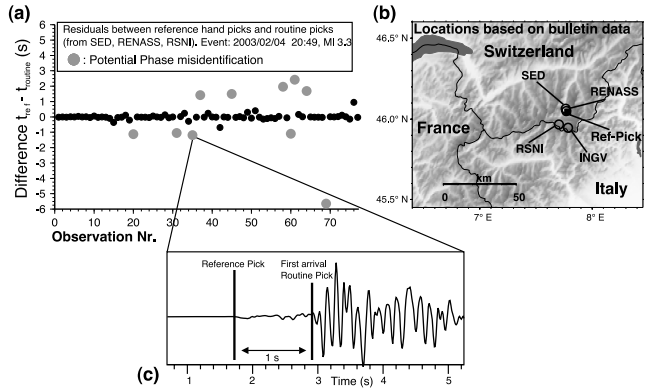

Figure 1. Example of phase misidentification in routine phase data. (a) Difference between (revised) reference hand picks and routine picks provided by SED (Switzerland), RENASS (France), and RSNI (Italy). Grey dots indicate probable phase misidentifications in routine phase data. (b) Locations of the same earthquake, as reported in different national and regional bulletins. 'Ref-Pick' denotes location resulting from reference picks and regional minimum 1-D model. (c) Waveform and corresponding routine and reference picks for an obvious phase misidentification. The routine pick is located at the secondary Pg phase.

the entire Alpine orogen requires data of more than 10 national and regional permanent networks (e.g. Solarino *et al.* 1997; Lippitsch *et al.* 2003). Merging such a heterogeneous data set presents several difficulties, since no common error assessment for timing and phase interpretation is available. Furthermore, identification of common events can be difficult because of significantly different hypocenter locations (Solarino *et al.* 1997). Fig. 1 denotes examples of inconsistencies and obvious phase misidentifications in routine phase data of several networks in the Alpine region, which may result in errors up to several seconds. To benefit from recent improvements in the quantity and quality of seismic stations (digital transmission, high sampling rates, accurate timing with GPS-systems, increasing number of broadband sensors, etc.), the existing inconsistencies in seismic phase data must be significantly reduced.

Due to the steadily increasing amount of available digital waveform data, automatic picking algorithms are required to measure phase arrival times with a high level of consistency for large data sets. Several automatic approaches have been developed over the past decades. Traditionally, characteristic functions from STA/LTA ratios of energy, envelopes, frequency, and particle motion are used to detect and pick the onset of a seismic phase (e.g. Allen 1978, 1982; Baer & Kradolfer 1987; Earle & Shearer 1994; Withers *et al.* 1998). More recently, autoregressive (AR) pickers based on the Akaike information criterion (AIC, Akaike 1973) were developed as described, for example, in Takanami & Kitagawa (1988) or Leonard & Kennett (1999). Usually, implementations of AR–AIC pickers have to be combined with phase detectors from STA/LTA ratios (e.g. Sleeman & van Eck 1999; Leonard 2000) or other techniques such as wavelet analysis (Zhang *et al.* 2003).

To enhance the consistency of phase picks of similar or repeating events (e.g. swarms) waveform-correlation can be used as described, for example, by Aster & Rowe (2000) and Rowe *et al.* (2002). Primarily, waveform-correlation provides only relative arrival times. Absolute arrival times can be obtained from applying an AR–AIC picker to a stack of aligned waveforms of a specific cluster as shown by Rowe *et al.* (2004). Such refined and adjusted phase picks provide an excellent base for high-resolution relocation of seismic sources (e.g. Rowe *et al.* 2004) and tomography studies (e.g. Satriano *et al.* 2008). Since correlations-pickers assume waveform similarity, their application is mainly limited to repeating seismicity at local scales.

Although accuracy of automatic picks is comparable to manual picks as demonstrated, for example, by Sleeman & van Eck (1999), Leonard (2000) or Zhang *et al.* (2003), most of the existing algorithms do not provide an assessment on the absolute uncertainty of the automatic pick. Since consistent data quality weighting is crucial for most traveltime inversions, the automatic error assessment represents an essential component of the phase picking procedure. Among the existing methods, the 'MannekenPix' (MPX) picking software (Aldersons 2004) is one of only a few algorithms that include an automatic quality weighting. Di Stefano *et al.* (2006) applied the MPX picking system successfully to the data of the Italian national seismic network.

To achieve an appropriate aperture to resolve the deep crustal structure of the Alps at a regional scale, a data set derived from several seismic networks has to be compiled. Furthermore, the low seismicity of this region requires data from a long recording period. Consequently, this results in a rather heterogeneous data set in terms of waveform characteristics and hypocentral information. The lower seismicity also demands more of the automatic picking and classification procedure, since a simple discrimination of very good from bad picks, as is typically done when automatic picking is used, would not be sufficient to provide enough phase picks.

In this work, we first present a consistent picking and error assessment for local and regional *P*-phases and identify common problems and inconsistencies in routine hand picking. Subsequently, we will give a brief introduction to the general concept of MPX and present calibration procedures suitable for local to regional scales. These procedures are applied to the greater Alpine region and the resulting high-quality automatic phase picks are inverted for 3-D velocity structure. The comparison with regional tomography models based on routine phase data extracted from the ISC Bulletin demonstrates the potential improvement of our re-picking approach.

2 ROUTINE HAND PHASE PICKING

Although traveltime based earth models and hypocentral solutions strongly depend on the accuracy of phase data, the description of consistent phase picking has received little attention in the literature. Simon (1981), Kulhánek (1990) and Kulhánek (2002) provide a general overview about seismogram interpretation from local to teleseismic scales. They focus mainly on basic descriptions of phases observable in common seismograms. The assessment of timing uncertainty and phase interpretation, however, is barely discussed. The fundamentals of digital signal processing and their influence on onset properties are described, for example, in Seidl & Stammler (1984), Scherbaum (2001) and Scherbaum (2002). Among the few recent guidelines, the 'New Manual of Seismological Observatory Practice' (NMSOP) of Bormann *et al.* (2002) provides an introduction to basic picking principles for local, regional and teleseismic seismograms. Although they propose to quantify the onset-time reliability, a detailed description for consistent quality assessment is missing.

In the following section, we present a hand picking procedure, which includes a consistent quality assessment for timing uncertainty and phase interpretation. It is focused on crustal phases of local to regional distances, but its principles apply likewise to teleseismic observations.

© 2008 The Authors, *GJI*, **176,** 542–554
Journal compilation © 2008 RAS

2.1 Phase timing and the assessment of its uncertainty

The basic quantities associated with a picked phase are usually the absolute arrival time and the corresponding observation uncertainty. Common qualification of timing uncertainties differentiate signals into 'impulsive' and 'emergent' phase onsets as, for example, used by the International Seismological Center (ISC). Such qualitative error assessment, however, no longer satisfy the resolution capability of modern digital waveform data. In addition, it is difficult or even impossible to give a general predictive definition of a seismic onset time, which could be used for the actual measurement of first arrival time from a sampled band-limited signal in the presence of noise (Seidl & Stammler 1984).

Consequently, a physical consistent formulation can only be achieved by a probabilistic point of view as suggested, for example, in Bormann *et al.* (2002). Such an approach directly relates the measured arrival time with the corresponding observation uncertainty. Considering the onset of a seismic phase as a probabilistic function $P_a(t)$, the arrival time is expressed as the 'most likely' time t_A, with $P_a(t_A) = \mathrm{Max}\,(P_a)$. On the other hand, the 'earliest' possible time for the phase onset is defined as t_E, where the likelihood for onset is approaching zero. Thus $P_a(t_E) \geq 0$. Similarly, the 'latest' possible time for the phase onset t_L, is defined as $P_a(t_L) \geq 0$. Fig. 2 illustrates the proposed concept in further detail. Although the onset of the phase (mainly characterized by a change in amplitude) is rather impulsive and exhibits an almost ideal signal-to-noise (SN) ratio, it is difficult to determine an arrival time consistent with picks of waveforms from the same seismic source recorded at other stations. The thick grey band between position '1' and '2' defines the time window that definitely includes the onset of the wavelet, while position '1' is certainly too early to be picked as t_E and '2' is too late as t_L. The band outlined by two broken lines denotes the possible threshold of the noise amplitude (arbitrarily defined as 1.5 times pre-signal amplitude).

In practice, we first determine the position of t_L and t_E. For a consistent determination of t_L and t_E, we have to setup a common procedure. Since the amplitude exceeds the threshold several times at position '2', the end of the grey band is certainly too late to be picked as t_L. Therefore, we define the intercept between signal amplitude and the *a priori* noise threshold as t_L. Usually, the consistent determination of t_E is more difficult. In Fig. 2 we fit a tangent (dashed line 'a') to the slope of the onset. If we shift the tangent from t_L towards earlier times, the slope decreases. The earliest possible time t_E corresponds to the first zero slope from t_L towards earlier time. Therefore, the start of the grey band (position '1') is certainly too early, whereas t_A would be too late to be picked as t_E. To ensure t_E includes the zero slope time in the presence of higher background noise, we could shift it earlier by approximately half the dominant noise period. Subsequently, we pick the arrival of the phase at the most likely position t_A, within the error interval of t_E and t_L (e.g. on the seismogram's leading edge). For the special case of a delta-pulse, t_E and t_L would coincide with t_A. In addition, a quantitative weighting scheme has to be defined where the assigned discrete weighting classes depend only on measured time error intervals ($t_L - t_E$). This procedure allows the adjustment of the weighting class definitions even after the picking process, whilst remaining consistent.

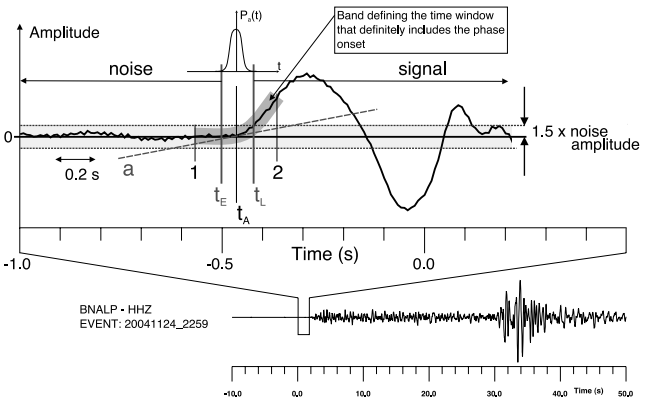

Figure 2. Probabilistic phase picking approach: the 'earliest' possible pick corresponds to t_E, the 'latest' possible pick corresponds to t_L. The most likely arrival time t_A is located within this interval. Primarily amplitude is used for the determination of t_E and t_L. See text for further details.

2.2 Phase identification and the assessment of its uncertainty

Although phase misinterpretation can result in significantly large errors (as demonstrated in Fig. 1), phase identification is typically not supplied with any observation error or uncertainty attribute at all (unlike the arrival time of a phase). Particularly for local earthquake studies in orogenic areas with significant lateral crustal structure variations, phase identification can become ambiguous. As an example, Fig. 3 presents a velocity reduced record section of a local earthquake near Walenstadt, Switzerland, with a focal depth of 13 km. Based on waveform characteristics alone, phase interpretation appears rather difficult for some stations in the distance range of phase triplication (e.g. SPAK and SIERE). In addition, the amplitude ratio between *Pg* and *Pn* exhibits strong variations between some stations (e.g. EMV and HEI) probably due to 3-D Moho topography. In these cases, *Pn* is likely to be missed and *Pg* will be picked as first-arrival phase.

Since most applications like hypocentral localization and traveltime tomography are still based on first-arrivals only, we have to setup an error assessment for phase identification to avoid such gross inconsistencies. For use in routine first-arrival studies and subsequent special studies, we define an error assessment for phase identification as shown in Table 1. In addition, synthetic traveltime curves for main crustal phases (as demonstrated in Fig. 3) can be used to identify phases or cross-check phase interpretations. Inconsistent picking of arrival times and phase identification can also bias the determination of first motion polarities and therefore directly affects the quality of fault plane solutions.

2.3 Sources of inconsistencies in routine picks

Besides insufficient error assessment of timing and phase identification, the picking procedure itself can induce a significant amount of inconsistency, which can result in errors up to several hundred milliseconds. A prominent example is the random choice of window size and amplitude scaling in phase picking (Douglas *et al.* 1997). Another common problem is the inconsistent usage of filters and misinterpretation of artefacts caused by digital filters. The application of acausal anti-aliasing filters in modern recording systems as described in Scherbaum (2001) can lead to oscillations prior to impulsive onsets often interpreted as precursory phases.

Such inconsistencies can be reduced by using pre-defined window lengths for picking, uniform amplification of amplitudes, and consistent application of filters. For reference picking of *P*-phases we used a 1 Hz 2nd order high-pass (HP) filter for broad-band

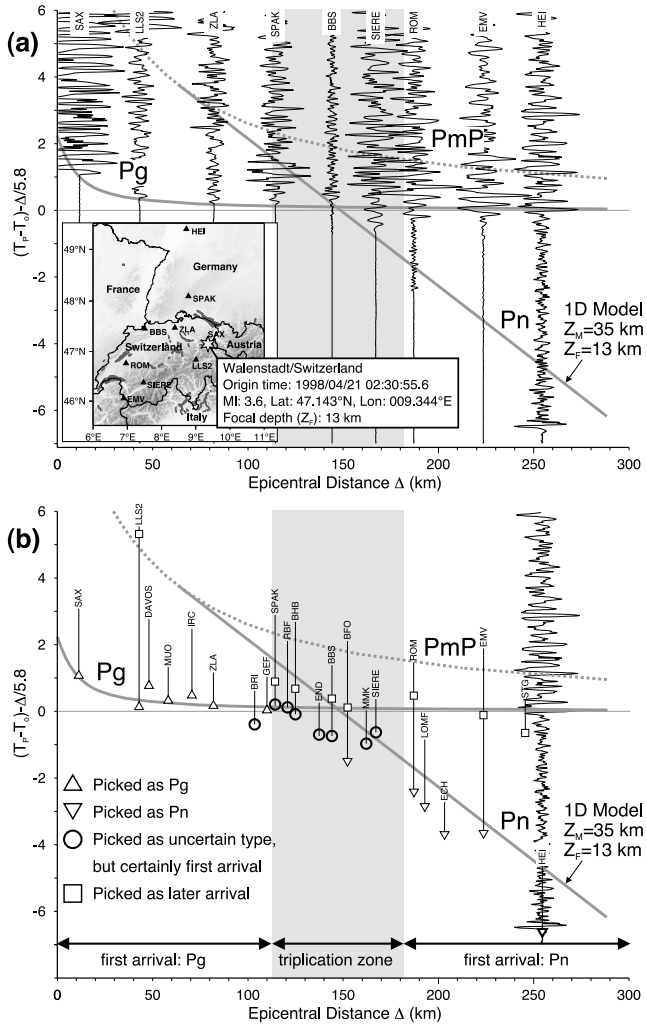

Figure 3. (a) Velocity reduced record section of a local earthquake near Walenstadt, Switzerland. Amplitudes are normalized to maximum amplitude of each trace. Synthetic traveltime curves for *Pg*, *Pn* and *PmP* are indicated by solid and dashed lines. Discrimination of phase type purely from waveform characteristics might be difficult for stations in triplication range (e.g. SPAK and SIERE). Denote differences in amplitude ratio between *Pg* and *Pn* for station EMV and HEI. Deviations between expected and observed *Pn* arrival are related to 3-D Moho topography. (b) Velocity reduced phase picks, crosschecked against synthetic traveltime curves derived from a simplified crustal model.

Table 1. Glossary used for phase identification of *P* and *S* waves at local to regional distances. The glossary implies a first order uncertainty assessment for phase identification.

Phase label	Phase is . . .	Phase used for routine 1st arrival studies
Pg, Sg	Direct (crustal)	Yes (if first arrival)
Pn, Sn	Moho-refracted	Yes (if first arrival)
PmP, SmS	Moho-reflected	No
P1, S1	Unknown type, but certainly first arrival	Yes
P2, S2	Unknown type, second arrival	No
P3, S3	Unknown type, third arrival	No
P, S	Unknown type, uncertain if first arrival	No

data in order to simulate a short period transfer function. Short period data is only HP filtered if obvious low frequency noise is present. Low-pass (LP) filters are only applied if significant high-frequency noise is observed. LP filters can also be used to somewhat attenuate precursory oscillations caused by acausal anti-aliasing filters.

3 AUTOMATED RE-PICKING OF *P*-PHASE DATA: APPLICATION TO THE GREATER ALPINE REGION

3.1 Local earthquake data set of the Alpine region

Waveform and bulletin data from about 1500 events with $M_l \geq 2.5$ recorded between 1996 and 2007 were compiled from 13 national and regional networks in the Alpine region. Waveforms provided by the different networks were all converted to common GSE2-format (Group of Scientific Experts, Geneva, 1990). Obvious timing and polarity problems present in some data were checked for and—where possible—corrected or the data were removed. To avoid inconsistencies in terms of station codes and station coordinates, information provided by the networks were compiled to a master station list similar to the procedure described by Solarino *et al.* (1997). The resulting data set comprises of more than 70 000 seismograms recorded at about 400 stations shown as triangles and circles in Fig. 4. This data set represents a unique compilation of digital waveforms from local earthquakes within the Alpine region. From this data set we select a reference data set consisting of a subset of 39 events, representative of the different tectonic regions and the range of magnitudes and focal depths. These reference events (locations indicated by white stars in Fig. 4) were consistently and accurately hand picked with the above described routine picking procedure. Table 2 shows the weighting scheme used for reference *P*-phase picking and the number of *P*-picks in each class. Epicentral distances for reference picks vary between 1 km and about 700 km.

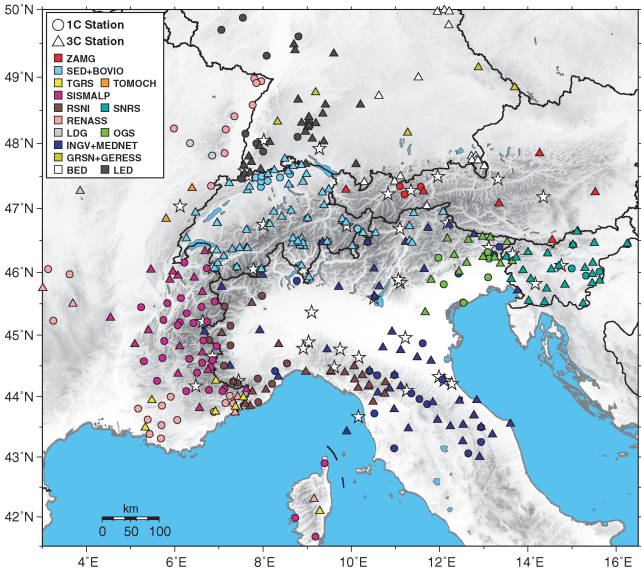

Figure 4. Networks and stations in greater Alpine region used in this study. Triangles denote three component stations, circles denote one component (vertical) instruments. Colours indicate the corresponding network affiliation. Not all of the stations operated at the same time. Additional white stars indicate location of reference events used for calibration of MPX.

Table 2. Error assessment used for reference *P*-phase picking and number of *P*-picks for each quality class derived from 39 reference events.

P-Quality class *qP*	Error ε_{qP} (s)	Weight (per cent)	# Observations
0	± 0.050	100	755
1	± 0.100	50	905
2	± 0.200	25	876
3	± 0.400	12.5	481
4	> 0.400	0.0 (rejected)	769

We used this reference data set for MPX calibration and test of the calibration scheme.

3.2 The MPX picking system

The concept of MPX is described in detail by Aldersons (2004) and Di Stefano *et al.* (2006). Here, we summarize only the basic principles of the algorithm. Although more recent versions of MPX are not limited to repicking, the version we used was designed only for repicking. As such, it requires an initial pick to guide the picking engine to an approximate phase onset time. The initial pick can be provided by an existing routine pick or a predicted time from a theoretical traveltime curve. The latter assumes the existence of an appropriate regional velocity model (preferably a minimum 1-D model, e.g. Kissling *et al.* 1994) and an approximate hypocentral location. If routine picks are used as initial picks, we have to ensure that the number of gross misidentifications like the example in Fig. 1 is small.

The MPX picking algorithm represents an extended version of the robust Baer–Kradolfer picker (Baer & Kradolfer 1987). The threshold for the picker is derived in an adaptive way by comparing apparent noise and signal characteristics. A noise window and a signal window are centred around the initial pick and are separated by safety gaps g_N and g_S as demonstrated in Fig. 5. The length of the safety gaps mainly depends on the expected maximum difference between initial pick and actual phase onset. Large safety gaps allow picking even from imprecise initial picks. However, mispicks and misinterpretation of later phases as first-arrivals become more likely.

A pattern recognition scheme weights different waveform attributes (predictors) obtained in the time window around the automatic pick and classifies the pick in discrete quality classes. The corresponding weighting factors are called 'Fisher coefficients' (Fisher 1936, 1938), which have to be calibrated with a set of reference hand picks (reference data). A multiple discriminant analysis (MDA) is used to derive appropriate Fisher coefficients from the reference picks.

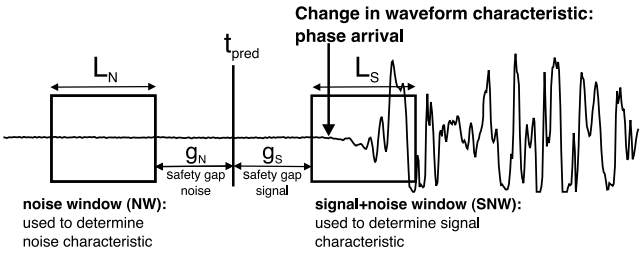

Figure 5. MPX search window configuration: The noise window *NW* and the signal+noise window *SNW* are centered around the initial pick (here predicted t_{pred}) and are separated by safety gaps g_N and g_S.

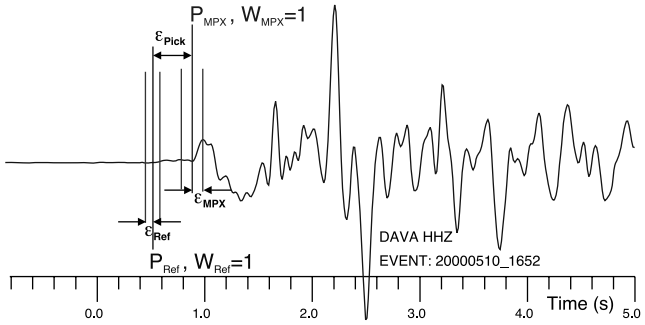

Figure 6. Example for misinterpretation of an impulsive later phase as first arriving *P*-phase by the automatic picker. Although automatic classification W_{MPX} corresponds to the reference weight W_{Ref}, the error $\varepsilon_{\mathrm{Pick}}$ between automatic and reference pick is several times larger than the error $\varepsilon_{\mathrm{MPX}}$ associated with quality class W_{MPX}.

3.3 Calibration of the automatic weighting procedure

The data set of 39 reference events was used to derive appropriate Fisher coefficients for automatic quality classification. The MDA compares the predictor values around the automatic pick with the associated reference quality class. The Fisher coefficients represent the optimum weighting of each predictor to estimate the corresponding quality class membership. This relationship between predictors and reference quality class is based on the assumption that automatic and reference picks are located at the same phase. However, the autopicker often misses the first-arrival and picks a later more impulsive phase as shown in the example of Fig. 6. To account indirectly for phase misinterpretation, we associate the predictors with a 'target' class instead of the reference class in the MDA. The 'target' class coincides with the reference class if the error $\varepsilon_{\mathrm{Pick}}$ between automatic and reference pick is within the error interval of the reference class. If it is larger, the 'target' class corresponds to the next lower class, where the error interval includes $\varepsilon_{\mathrm{Pick}}$ analogous to the procedure described by Di Stefano *et al.* (2006). However, this will result in a larger number of actual high-quality picks downgraded to lower classes by MPX.

In addition, the choice of reference picks used for the MDA can have a significant influence on the Fisher coefficients and the stability of the resulting automatic classification. Subsets dominated by higher quality picks result in a conservative but robust error assessment in our tests. Fisher coefficients derived from a subset of reference events with $M_l \geq 4.0$ are given in Table A1 of Appendix A. This magnitude threshold leads to an average quality that is biased towards higher SN ratios, since first arriving *Pn* and *Pg* phases at distances ≥100 km have SN ratios comparable to first arriving *Pg* phases at distances <100 km.

Fig. 7 illustrates the performance of the corresponding weighting scheme in terms of accuracy and classification when applied to all reference events. N_{ij} denotes the number of picks of reference class *i* classified by the pattern recognition scheme as automatic class *j*. The σ_{ij} represent the standard deviation for differences between reference picks of class *i* and corresponding automatic picks of class *j*. A satisfactory automatic picking and quality assessment is achieved if the deviation between automatic and reference picks is within the error interval of automatic quality classification ($\sigma_{ij} \leq \varepsilon_j$) and if only few low quality reference picks are moderately upgraded to higher quality classes by MPX. However, upgrades from worst to top quality classes lead to a serious distortion of the data error estimate for seismic tomography and may generate artefacts in tomographic images. Both requirements are satisfied

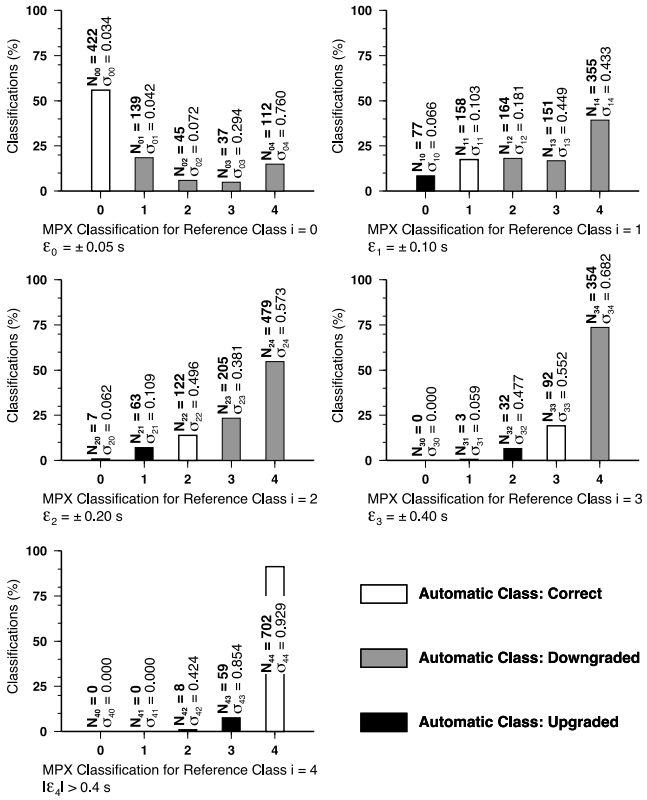

Figure 7. Performance of MPX for a weighting scheme derived from reference events with $M_l \geq 4.0$. The N_{ij} denote the number of picks of reference class *i* classified by MPX as automatic class *j*. The σ_{ij} represent the standard deviation for differences between reference picks of class *i* and corresponding automatic picks of class *j*. White bars indicate correct classification, gray bars indicates downgrading, and black bars identify upgrading of picks by MPX. The automatic weighting classifies more than 55 per cent of the class '0' picks correctly. For classes ≥1 MPX downgrades a large number of picks to lower or lowest classes.

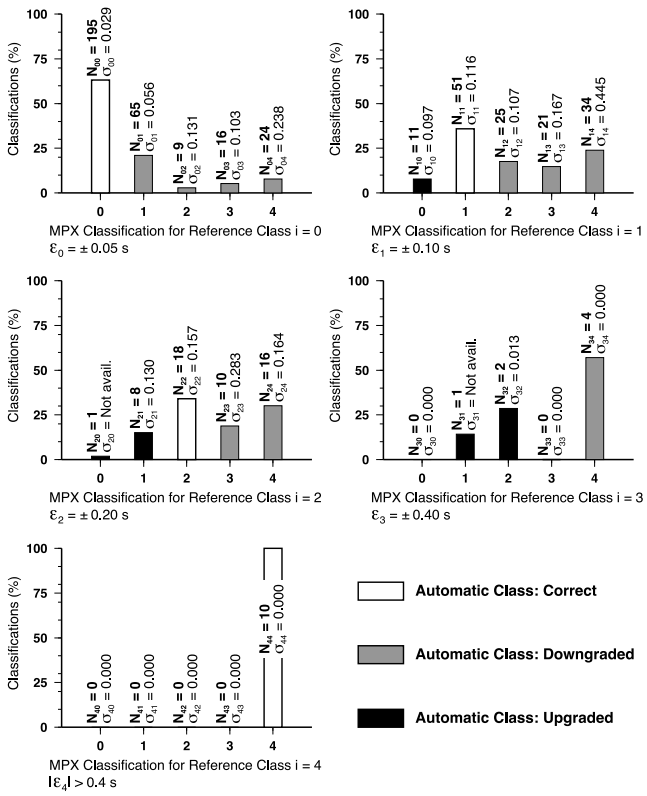

Figure 8. Performance of MPX for epicentral distances < 100 km (predominantly *Pg* phases) similar to Fig. 7. The used weighting scheme is derived from reference picks with $\Delta < 100$ km.

for automatic class $j = 0$ and 1 for the weighting scheme in Fig. 7. All σ_{ij} are less than or close to ε_j and none of the reference class '4' picks (rejected class) are upgraded to high-quality class '0' or '1'. For this weighting scheme, automatic picks of class '0' and '1' satisfy the requirements for use in tomographic inversion.

The weighting scheme derived from using 'target' classes and reference picks of stronger events results in a robust but rather conservative classification. This procedure is necessary to minimize the number of misidentifications present especially at larger regional distances where weak emergent Pn phases are followed by impulsive *Pg* or *PmP* phases. In addition, the generally lower SN ratio increases the likelihood of mispicks at these distances.

For short distances dominated by first arriving *Pg* phases we expect less complex waveforms and larger SN ratios. Fisher's coefficients given in Table A2 of Appendix A are derived from reference picks at epicentral distances $\Delta < 100$ km (dominated by first arriving *Pg* phases). The corresponding classification performance of MPX for distances < 100 km is shown in Fig. 8. The performance of the automatic classification is much higher for this distance range as indicated by the larger number of correctly predicted qualities (white bars). The σ_{ij} are less-equal or close to ε_j for all usable automatic classes (0–2) and none of the rejected picks of class '4' are upgraded to high-quality classes. Although most of the actual class '3' reference observations are rejected by MPX, we recover downgraded picks of class '0', '1' and '2' in the automatic class '3'. Since none of the quality class '4' picks are upgraded and all $\sigma_{i3} \leq \varepsilon_3$, automatic picks of class '0'–'3' can be used in this distance range. The higher recovery rate within this distance range can provide essential picks to reduce azimuthal gaps or to increase the number of observations per event and may allow the retention of otherwise rejected events.

Since *a priori* information about hypocenters exists, we calculate an approximate epicentral distance for each waveform. To achieve the maximum performance of MPX in the so-called 'production stage' (application of calibrated MPX to the complete data set) we split the data set into two parts: Fisher coefficients of Table A2 are used for $\Delta < 100$ km, whilst the robust coefficients of Table A1 are used for waveforms with $\Delta \geq 100$ km. With such a distance-dependant calibration scheme we achieve a first order discrimination between *Pg* and *Pn* phases. Accordingly, automatic picks of class 0-3 from the first part can be used for tomographic inversion, whereas, from the second part only class 0–1 have sufficient quality.

Fig. 9 summarizes the performance of MPX for three different calibration schemes using the matrix representation introduced by Di Stefano *et al.* (2006). Automatic picks are compared to reference picks similar to Figs 7 and 8. The number of reference picks of quality class *i* classified by the pattern recognition scheme as automatic class *j* is represented by N_{ij}. The total number of automatic picks classified as class *j* is described by N_j and the standard deviation for differences between automatic picks of class *j* and corresponding reference picks is indicated by σ_j. By using all reference picks for the MDA similar to the procedure suggested by Di Stefano *et al.* (2006), only automatic picks of class 0 satisfy the requirements for application in tomography (Fig. 9a). Automatic picks of class

© 2008 The Authors, *GJI*, **176,** 542–554
Journal compilation © 2008 RAS

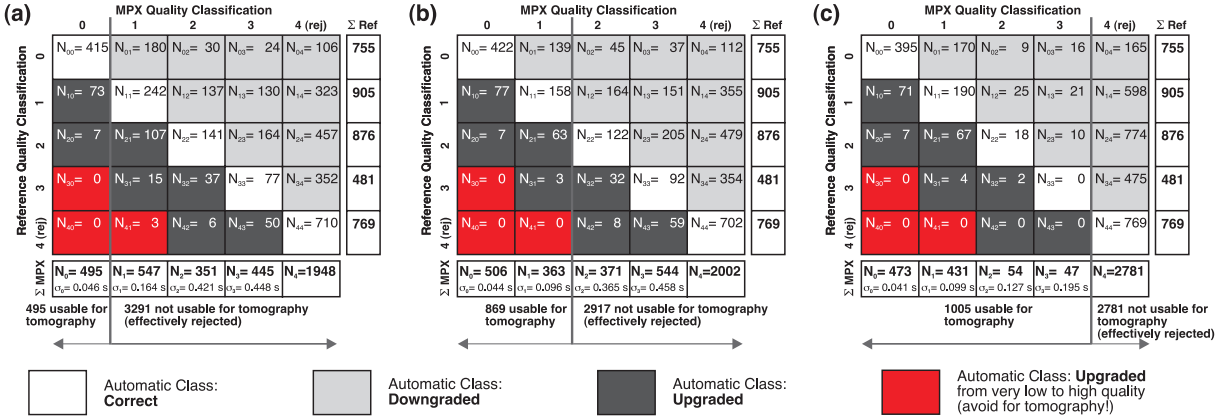

Figure 9. Performance of MPX for three different calibration schemes using a matrix representation. (a) Similar to Di Stefano *et al.* (2006), all reference picks are used for the MDA. For our data set, only automatic picks of class 0 satisfy the requirements for use in tomography (see text). (b) Only waveforms of events with $M_l \geq 4.0$ are used for the MDA. Automatic picks of class 0 and 1 can be used for tomography. (c) Distance-depending calibration as used in this work. Automatic picks of class 0–2 and, in this case, also class 3 (see text) can be used for tomography.

1 exhibit a standard deviation σ_1 significantly greater than $|\varepsilon_1| = 0.1$ s and in addition, they contain three picks upgraded from the lowest quality class 4.

In Fig. 9(b) only waveforms of events with $M_l \geq 4.0$ are used for the MDA. Automatic classes 0 and 1 can be used for tomography, which leads to a significantly increased number of picks. An even higher number of usable picks is obtained with the distance-dependant calibration scheme shown in Fig. 9(c).

3.4 Predicted arrivals for production mode

Since we do not have reliable routine picks for most of the waveform data, we can only rely on predicted arrival times as initial picks. This represents the standard case for most regional data sets. In a first run, we used the minimum 1-D model of Solarino *et al.* (1997) and catalog locations to calculate predict *P*-arrivals. Fig. 10(a) shows the differences between calculated predicted arrivals and corresponding reference picks ($tP_{\mathrm{pred}} - tP_{\mathrm{Ref}}$) for reference picks identified as first-arrivals (*Pg*, *Pn*, *P1*) and usable quality class. The differences show a broad scatter and the mean indicates a systematic bias of predicted arrival times. Since the model of Solarino *et al.* (1997) denotes a minimum for a similar area but a largely different data set of local earthquakes, the model predicts systematically biased arrival times indicated by the negative mean. The broad scatter in predicted arrivals requires the use of wide safety gaps, to ensure that the actual phase can be reached by the signal window *SNW*. Safety gaps of, for example, ±4.0 s result in a large number of mispicks, especially in the range of the crossover distance between *Pn* and *Pg*. To overcome this problem, the accuracy of predicted arrival times had to be improved.

In our approach, we first inverted the reference data set to derive a coarse regional minimum 1-D model as described by Kissling (1988). The model of Solarino *et al.* (1997) was used as initial model for the inversion. To improve and stabilize the station corrections of the minimum 1-D model, we extended the reference data set by using unweighted automatic picks. The low quality automatic picks were derived from the pure Baer–Kradolfer picker applied without any quality weighting to the complete data set of 1533 events. Hypocentres were relocated in the coarse minimum 1-D model and obvious mispicks were identified by residuals $|\delta t| > 2.0$ s. High quality events (azimuthal gap $< 100^\circ$, minimum number of observations = 20, rms ≤ 0.8 s) from this data set were combined with the reference data. In this combined data set, we kept the original weights for the reference picks and weighted all automatic picks by only 25 per cent to account for the lower quality. The combined phase data were used to derive the updated regional minimum 1-D model *s*07*b* and the corresponding station corrections by simultaneous inversion. The unweighted automatic picks were used to relocate all events within *s*07*b* (station corrections applied). Again, we removed all picks associated with residuals $|\delta t| > 2.0$ s and rejected low quality events with azimuthal gap $>180^\circ$, minimum number of observations <6, and rms >1.0 s. The remaining 930 events were selected for re-picking with the calibrated MPX in production stage. Fig. 10(b) shows the differences between predicted arrivals from model *s*07*b* (applied station corrections and relocated hypocenters based on unweighted automatic picks) and reference picks. The standard deviation is reduced by a factor of two and the significantly higher accuracy of the minimum 1-D model allows the use of narrower safety gaps.

3.5 Results of MPX production mode

As previously mentioned, we split the data set into two distance ranges and apply different sets of corresponding Fisher coefficients to each subset. Waveforms associated with distances $\Delta \leq 20$ km are LP filtered (15 Hz, 2nd order) to remove possible high-frequency precursors generated by acausal anti-alias filters. For $20 < \Delta < 100$ km we apply a HP filtered (1 Hz, 2nd order) to remove possible low-frequency noise. The same configuration of filters was used for the calibration of the weighting scheme shown in Fig. 8.

Non-seismic signals like spikes and step-functions (caused, e.g. by problems in transmission) are commonly present in large heterogeneous data sets. The identification of such signals is crucial for reliable automatic picking, since they are often misinterpreted as high-quality arrivals by the picking algorithms. To avoid mispicks due to quality problems present in the data set, we perform an automatic quality check around the predicted arrival time in a pre-picking stage and reject obvious low-quality seismograms. A de-spiking routine was used to to detect and remove possible spikes. Steps in the seismograms caused by data gaps filled with zeros are identified by an running average detector applied around the predicted arrival time.

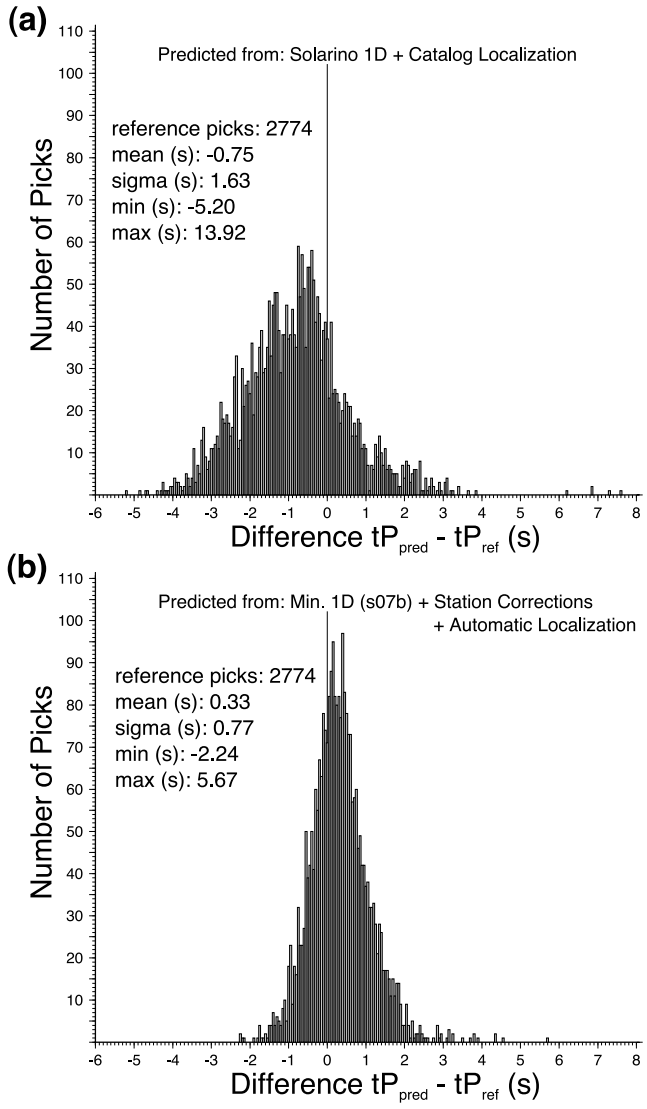

Figure 10. Difference between predicted and corresponding reference hand picks ($tP_{\rm pred} - tP_{\rm Ref}$). (a) Predicted arrival times calculated from the minimum 1-D model of Solarino *et al.* (1997) (obtained from a different data set) and catalog locations. (b) Predicted arrival times calculated with a true minimum 1-D model (specifically calculated for our data set) and usage of corresponding station corrections. Localizations used to derive predicted arrival times are based on unweighted automatic picks and are relocated in the same minimum 1-D model. Usage of a minimum 1-D model with station corrections and relocated hypocenters significantly improves the accuracy of predicted arrival times.

The final result of the production mode is summarized in Table 3. The upper part shows the number of automatic picks for each class after merging picks from all 930 events at both distance ranges. These picks were used to relocate all events in the minimum 1-D model *s*07*b*. After rejecting low-quality events with an azimuthal gap $> 180^\circ$ or less than 8 observations, 551 events were left. The middle part of Table 3 summarizes the number of automatic picks corresponding to the 551 events. The lower part of Table 3 shows the results if only one set of robust Fisher coefficients (1F) for the entire distance range is used. In this production mode we used the Fisher coefficients listed in Table A2. By splitting the data set into two distance ranges, we gain about 200 events and 4000 additional phases.

Table 3. Results of MPX production mode. Upper part: Number of automatic picks derived from all 930 events used for production mode with two distance-dependent sets of Fisher coefficients (2F). Middle part: Corresponding automatic picks left after removal of low-quality events (gap $> 180^\circ$ and $N_{\rm obs} < 8$). Lower part: Automatic picks of locatable events using only one set of robust Fisher coefficients for the entire distance range (1F).

2F All events (930)	
Class	# Autopicks
0	5793
1	5242
2	1191
3	1131
Σ	13 357
2F Locat. events (551)	
0	5046
1	4340
2	906
3	862
Σ	11 154
1F Locat. events (356)	
0	4746
1	2513
2	–
3	–
Σ	7259

Table 4. Final high-quality *P*-phase data set for the Alpine region consisting of MPX automatic picks and reference hand picks of 552 events.

Quality class *qP*	Error ε_{qP} (s)	# MPX+REF Picks
0	±0.050	5387
1	±0.100	4875
2	±0.200	1822
3	±0.400	1225
Σ		13 309

Finally, we merged the automatic picks with the extended reference data set (hand picks of 49 events). If an automatic and reference pick is available for the same observation, we replace the automatic by the reference pick, since its weighting is expected to be less conservative. The combined data set is then relocated in minimum 1-D model *s*07*b* one more time. To identify gross mispicks, travel-time residuals of $|\delta t| > 0.8$ s (twice the error of lowest usable class) were visually cross-checked against waveforms in a semi-automatic procedure. From 1373 cross-checked picks, 103 are identified as mispicks. After removing identified mispicks from the data set and a last check of event quality (gap $<180^\circ$, $N_{\rm obs} \geq 8$) 552 events remain. Table 4 summarizes the final high-quality *P*-phase data set for the Alpine region. The average picking error can be estimated from the number of picks for each class and the error interval of each class. For our final data set we obtain an average picking error of $\varepsilon_t \approx 0.12$ s with maximum errors not exceeding 0.8 s. The corresponding ray-coverage for the final data set is shown in Fig. 11. Reference events used for calibration of MPX are indicated by white stars and gray stars denote additional reference events.

© 2008 The Authors, *GJI*, **176,** 542–554
Journal compilation © 2008 RAS

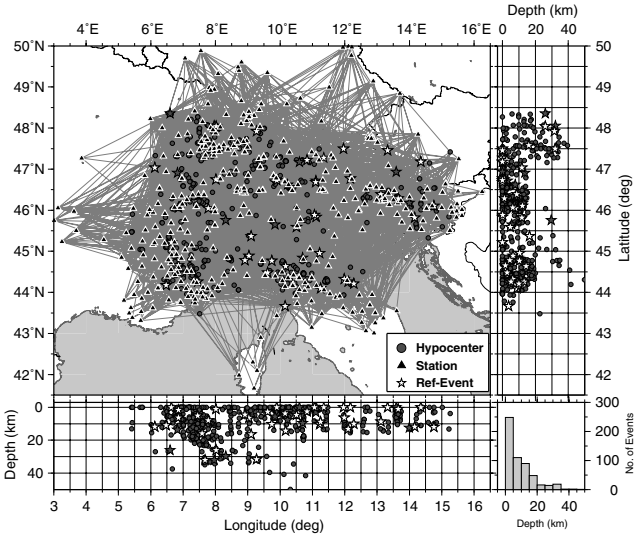

Figure 11. Ray-coverage of the combined high-quality *P*-data set consisting of 552 local earthquakes. Triangles denote stations, circles represent hypocenters, white stars indicate locations of reference events used for calibration of MPX (similar to Fig. 4), and gray stars denote additional reference events. Hypocenters correspond to locations in minimum 1-D model *s*12*c*.

4 LOCAL SOURCE TOMOGRAPHY WITH HIGHLY CONSISTENT DATA SET

The combined arrival times of the 552 well located events are used for local earthquake tomography. According to the procedure recommended by Kissling *et al.* (1994) we determine a regional minimum 1-D model, which will be used as initial model for the 3-D inversion.

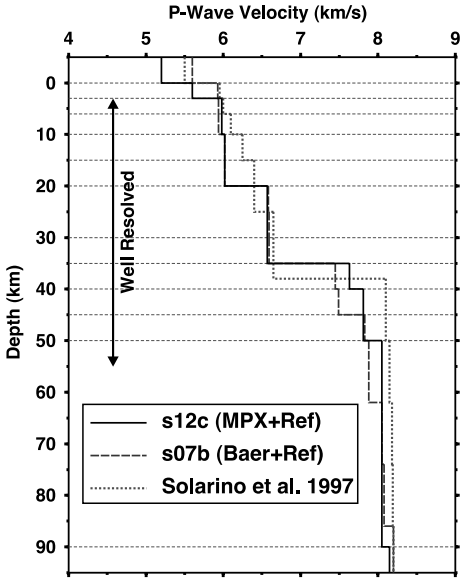

Figure 12. Different (minimum) 1-D Models for Alpine region. Dotted line indicates the regional model of Solarino *et al.* (1997) derived from merged phase data. Higher velocities within the upper and mid-crust reflect the influence of the Ivrea body in the western Alps. Model *s*07*b* (dashed line) is based on unweighted automatic picks mixed with reference hand picks. Model *s*12*c* is derived from MPX quality-weighted automatic picks mixed with reference hand picks.

4.1 Consistent minimum 1-D model for the alpine region

The regional minimum 1-D model is derived in an iterative inversion procedure as described by Kissling (1988). The initial model for the inversion is the preliminary model *s*07*b*, which is based on unweighted automatic picks and reference hand picks. The model is indicated by the dashed line in Fig. 12. The final high-quality regional minimum 1-D model *s*12*c*, based on quality-weighted automatic and reference picks, agrees quite well with *s*07*b* for the upper and mid crust. In the depth range of the lower crust to upper mantle (35–50 km) *s*12*c* indicates higher velocities. The lower velocities of *s*07*b* might result from the large number of delayed picks present in low-quality automatic picks. In such a procedure, weak *Pn* phases are often missed and later phases are therefore misinterpreted as first-arrivals, leading to lower velocities.

Fig. 13 presents the station corrections of the minimum 1-D model *s*12*c*. Station corrections express deviations from the 1-D model due to 3-D structure with respect to a reference station (e.g. Kissling 1988). The correction of the reference station is defined as zero. Negative corrections (circles) indicate higher velocities compared to reference station and positive corrections (crosses) indicate lower velocities. Corrections in a large regional model usually represent a mixture of site effects close to the surface (e.g. sediments) and Moho topography (especially for stations located at the edge of the network). Therefore, the detailed interpretation can become ambiguous whereas the general pattern of corrections is an indication of consistency of the phase data. The corrections of model *s*12*c* denote a very consistent and sensible distribution for the entire region. Station BNALP in the central swiss Alps was chosen as reference station. As expected, stations at the edge of the network dominated by mantle phases from a limited range of backazimuths denote negative corrections. This effect can add up to several seconds in places like southern Germany, where the Moho is much

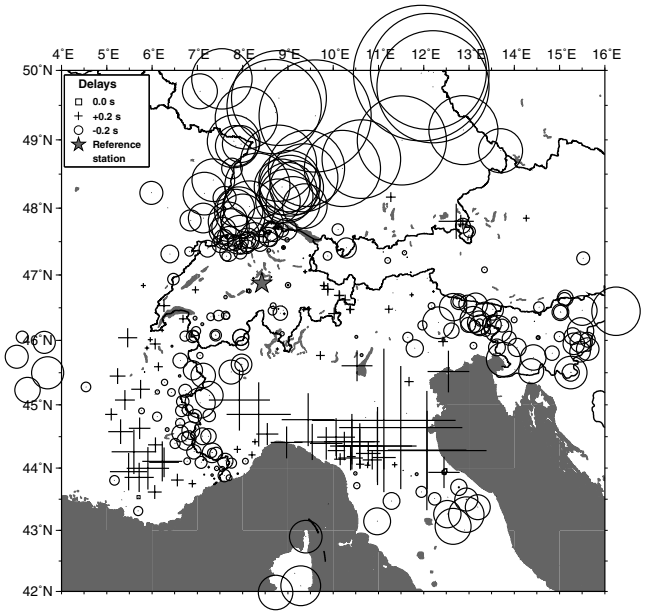

Figure 13. Station corrections of minimum 1-D model *s*12*c* for stations with at least five observations. Reference station BNALP is represented by a gray star. Negative corrections (circles) indicate higher velocities compared to reference station. Positive corrections (crosses) indicate lower velocities. Symbol size corresponds to correction amplitude.

shallower than the average value of 35 km indicated in model *s*12*c*. In addition, negative delays are observed throughout the western Alps, in the area of the Ivrea body, parts of the south-eastern Alps, and for massifs like the Black Forest. Positive delays associated with reduced velocities are mainly observed in the Provence area, within the Apennine Mountains, and throughout the Po plain. Station corrections in Switzerland and surrounding areas agree very well with the results obtained by Husen *et al.* (2003).

4.2 Preliminary 3-D results and comparison with ISC routine phase data

We inverted the high-quality data set of 552 events for 3-D structure using the SIMULPS14 code (e.g. Thurber 1983; Eberhart-Phillips & Michael 1993; Haslinger & Kissling 2001). Initial hypocenters and *P*-wave velocities were taken from *s*12*c*. The horizontal spacing of inversion nodes is 25 × 25 km and the vertical distance between node planes is 15 km. In-between these nodes, velocities are interpolated by the inversion code. The rather coarse parametrization turned out to be the finest possible parametrization without showing strongly heterogeneous ray coverage and results in a uniform resolution for major parts of the Alpine lithosphere. The left-hand column of Fig. 14 shows horizontal cross sections through the preliminary 3-D model at two different depths.

The Bulletin of the ISC represents the largest compilation of routine phase picks reported by seismological agencies around the globe and therefore allows the direct comparison between routine data and repicked data at regional scales. All events extracted from the ISC Bulletin (about 10 000 between 1996 and 2007) were relocated in the minimum 1-D model *s*12*c* prior to the 3-D inversion. As demonstrated, for example, by Grand (1990), Spakman *et al.* (1993) or Röhm *et al.* (2000), ISC phase data contain a considerable amount of random and systematic errors up to the order of minutes. Therefore, *P*-phases indicating traveltime residuals $|\delta| > 5.0$ s are considered as outliers and were removed from the data set. Subsequently, all remaining phases were used to relocate the events again. Finally we selected well-locatable events with at least 10 *P*-phase observations and an azimuthal gap $<150^\circ$. The remaining data set consists of about 95 000 *P*-phases from 3400 events in the Alpine region. Hence, the ISC data set includes about six times more events and about seven times more phases than our repicked data set. Based on the study of Röhm *et al.* (2000) we estimate the

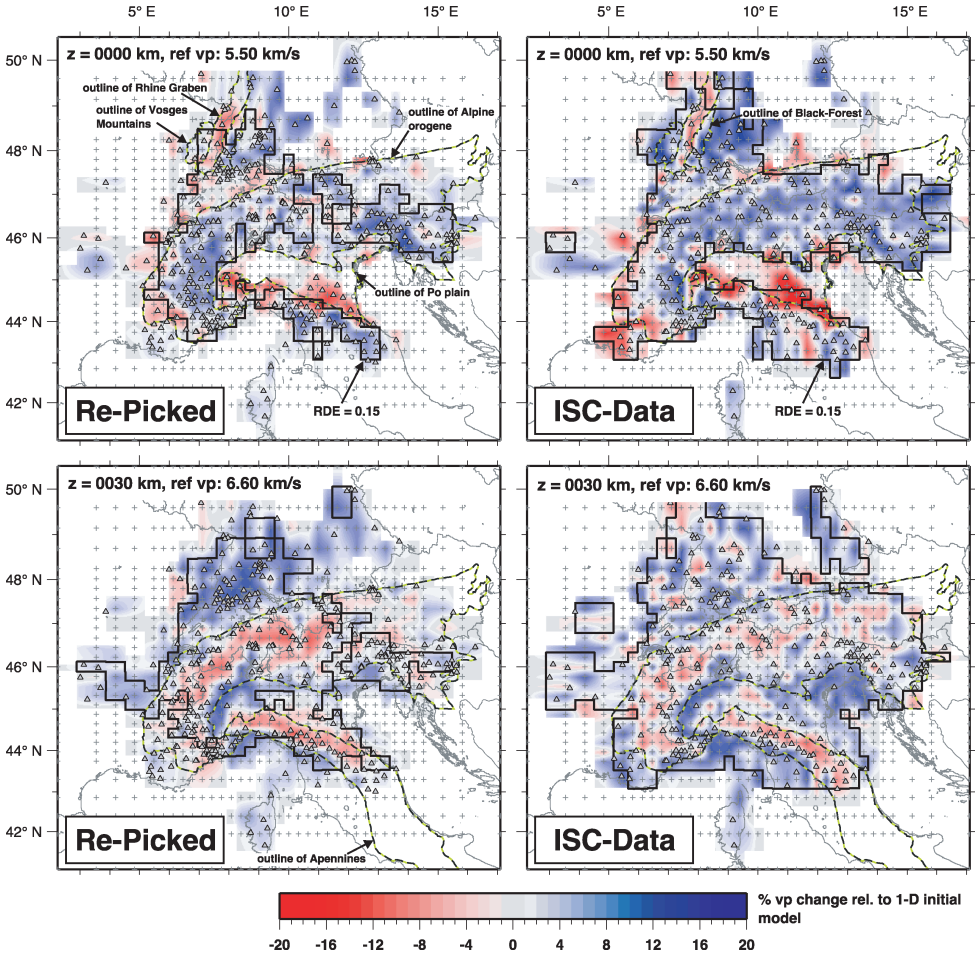

Figure 14. Comparison of tomographic images based on high-quality re-picked phase data (left-hand column, total of 13 300 *P*-phases with an average estimated timing error of 0.12 s) and standard ISC phase data (right-hand column, total of 95 000 *P*-phases with an average estimated timing error of at least 0.3 s) at 0 and 30 km depth. The v_P velocity structure is shown as percentage change relative to the 1-D initial reference model (same for repicked and ISC). Bold black contours outline resolution diagonal element (RDE) of 0.15 and green-black dashed lines outline major tectonic units as indicated. Triangles denote location of stations and crosses denote inversion grid nodes. Note how the tomographic image of 30 km depth obtained from repicked phase data is much more reliable in the well-resolved region—showing much fewer single cell anomalies of checkerboard type—while for very shallow depth, the performance of the two data sets is virtually the same with the larger ISC data set resolving a significantly larger region.

© 2008 The Authors, *GJI*, **176,** 542–554
Journal compilation © 2008 RAS

minimum average timing error of the filtered data set to be in the order of 0.3 s.

We used the same initial model and the same inversion parameters (damping value 100, five iterations, RK*P*-ray tracing) for the 3-D inversion of the ISC data set as we used for the re-picked data. The right-hand column of Fig. 14 shows the corresponding cross-sections through the ISC based 3-D model. The bold black contours in Fig. 14 outline the resolution diagonal element (RDE) of 0.15, which is used as a first order assessment of the solution quality in both models.

The uppermost part of the model seems to be rather well resolved by ISC data set (Fig. 14, 0 km depth) due to the higher data coverage compared to the repicked data set (indicated by enlarged area of RDE = 0.15 in the ISC data). Tectonic units like massifs (Black–Forest, Vosges mountains), sedimentary deposits (southern Rhine Graben, Po plain, partly Molasse basin), and the Alpine orogen are clearly resolved by the ISC data. The higher noise level of the ISC data becomes obvious in 30 km depth (Fig. 14), where the crustal root of the Alps and the northern Apennines are much more clearly imaged by the repicked data set. The tomographic image derived from the ISC data shows only few coherent structures and, in addition, it denotes a multitude of checkerboard type single cell anomalies where a smooth *P*-wave structure is expected. The reduced resolution of the ISC data in the deeper part of the model might result from the increased number of inconsistently picked or misidentified regional *Pn* phases.

Considering the higher noise level of the ISC data, stronger damping might be in order and this would likely reduce the amplitude of single cell anomalies that lead to the checkerboard appearance. This, however, would obviously also reduce the amplitude of the fair and well resolved anomalies making any interpretation of deep structure such as the Alpine crustal root even more difficult. In conclusion, ISC data is of significantly lower quality than our compiled and selected local earthquake data set and higher quality data leads to better resolution. Neither of these conclusions comes as a surprise.

4.3 Consistency of repicked data set

The consistency of the preliminary 3-D model is demonstrated in Fig. 15. The $v_P = 7.25$ km s^{-1} iso-surface (grey colour code) of the 3-D model is compared with the Moho topography from Controlled Source Seismology (CSS) modeling of Waldhauser *et al.* (1998). Topography of the CSS model is indicated as coloured contour lines, representing European-, Adriatic- and Ligurian–Moho. The dashed line in Fig. 15 outlines the well-resolved parts of the 3-D model. Poorly resolved or unresolved areas are masked. The tomographic model agrees very well with the CSS model for the major parts of the region. We observe steep gradients in the western Alps and a wider trough in the eastern Alps. Crustal roots below the Alps and the Apennines are pronounced features. Furthermore, we compared the tomographic model with the recent receiver functions study of Lombardi *et al.* (2008). The colour of the triangles in Fig. 15 represent Moho depth derived from a grid-search technique. Results of both methods show a high degree of agreement.

5 DISCUSSION AND CONCLUSION

Compilation of high-quality phase data for regional tomography typically requires the repicking of seismograms, since routine picks contain a large number of mispicks. In addition, error assessment of merged routine data is usually inconsistent. A uniform assessment of phase identification and timing uncertainty, however, is essential for traveltime inversion. The routine hand picking procedure presented in this work leads to highly consistent phase picks and allows a flexible quality weighting. Since the error intervals of the onsets (defined by t_E and t_L) are explicitly picked, the weighting scheme can be adjusted posterior to the picking, if necessary.

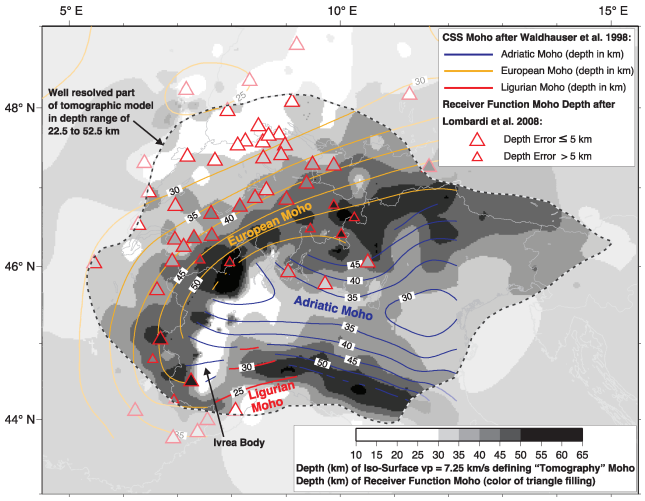

Figure 15. Moho topography derived from iso-surface of $v_P = 7.25$ km s^{-1} in our preliminary 3-D model. Contour lines indicate Alpine Moho derived from CSS after Waldhauser *et al.* (1998). Colour code of triangles denote Moho depth from receiver function study of Lombardi *et al.* (2008). The dashed line outlines the well-resolved parts of the 3-D model.

Considering the amount of waveform data necessary for regional studies, hand picking does not represent a feasible alternative to automated repicking approaches. The MPX picking system provides quality-weighted automatic picks with an accuracy and consistency comparable to manually picked data. Automatic quality classification achieved by the MDA leads to excellent assessment for picks at local distances (*Pg* phases exclusively) but only a satisfactory assessment for mixed picks at local to regional distances. By splitting the data set into two distance ranges and by using a regional minimum 1-D model, we achieve a first order discrimination between *Pg* and *Pn* phases. Therefore, different settings for MPX (Fisher coefficients and waveform filters) have to be used for the two subsets. For reliably picking *Pn* phases, a more conservative weighting scheme avoids misidentification of later arrivals, though the conservative weighting results in a smaller recovery rate of medium quality picks. The separate treatment of *Pg* and *Pn* phases during automated picking and subsequent merging of picked phases leads to a significantly increased number of automatic picks of high overall assessment quality. The good agreement between the reference and these automatic picks indicates that the phase association is correct for the majority of picks.

To further improve the performance of MPX, an automatic assessment of the various phase onsets will have to be included in the picking algorithm, since the MDA cannot account for it directly. As any other such algorithms, MPX picks the earliest well-defined signal as the first arriving phase. However, beyond the crossover distance the first arriving *Pn* is often less well-defined than secondary arriving phases such as *Pg* or *PmP*. To correctly identify the picked phase multiple picking approaches, as suggested by Bai & Kennett (2000), have to be considered. They propose the use of attributes provided by short- to long-term average ratios, autoregressive

modeling and polarization analysis to pick and identify series of *P*- and *S*-phases.

The iterative use of an automatic picker and minimum 1-D models are necessary to obtain consistent sets of regional phase data, since the accuracy of the automatic picks strongly depends on the reliability of predicted arrival times. Particularly for locations in-between networks, catalogue locations provided by agencies can differ significantly from the true location. In addition, 3-D structure as expected in an orogen region requires the use of station corrections.

The combined data set of reference picks and quality-weighted automatic picks suggests an average picking error of about 0.12 s. In combination with a 3-D model parametrization of 25 × 25 × 15 km, the average accuracy allows the resolution of at least 5 per cent *P*-wave perturbations in the mid crust. The 1-D inversion of the combined data leads to a robust regional minimum 1-D model with rather consistent station corrections, reflecting subsurface geology and Moho topography of the Alpine region. Results of the preliminary 3-D inversion indicate satisfactory lateral resolution for about 80 per cent of the Alpine arc. The resolution in depth encompasses the entire crust and the uppermost mantle up to depths of 50–60 km for the most parts of the Alps. The Moho topography derived from the iso-surface of $v_P = 7.25$ km s^{-1} in the preliminary 3-D model agrees very well with models from CSS and recent receiver function studies.

The comparison between repicked phase data and routine picks extracted from the ISC Bulletin clearly demonstrates the impact of a high-quality data set on the resolution and reliability of the tomographic image. The resolution of lower crustal structures with local earthquake tomography requires a consistently picked data set. Inconsistencies in picking and the lack of a common quality assessment cannot be compensated by an increased quantity of phase data.

ACKNOWLEDGMENTS

We are grateful to the following networks who provided us with digital recordings and bulletin data used in this study: BED (Ludwig-Maximilians-University, Munich), GERESS (Hannover), GRSN/SZGRF (Erlangen), INGV/MEDNET (Rome), Landes-Erdbebendienst (Freiburg i. B.), OGS/CRS (Udine/Trieste), RENASS (Strasbourg), RSNI/DipTeris (Genova), SED (Zurich), SISMALP (Grenoble), SNRS (Ljubljana), TGRS (Nice) and ZAMG (Vienna). Furthermore, we thank the ISC for their tremendous effort in collecting arrival times in the ISC Bulletin.

The reference picking was performed with the 'SeismicHandler' package (Stammler 1993). Most of the plots were generated using the Generic Mapping Tool by Wessel & Smith (1995). We thank C. Rowe and F. Waldhauser for their constructive reviews, and Manfred Baer and Ben Edwards for their helpful comments and proof-reading.

REFERENCES

Akaike, H., 1973. Information theory and an extension of the maximum likelihood principle, in *2nd International Symposium on Information Theory,* pp. 267–281, eds Petrov, B.N. & Csaki, F., Akademiai Kiado, Budapest.

Aldersons, F., 2004. Toward three-dimensional crustal structure of the Dead Sea region from local earthquake tomography, *PhD thesis*, Tel Aviv University, Israel.

Allen, R.V., 1978. Automatic earthquake recognition and timing from single traces, *Bull. seism. Soc. Am.,* **68,** 1521–1531.

Allen, R.V., 1982. Automatic phase pickers: their present use and future prospects, *Bull. seism. Soc. Am.,* **72,** S225–S242.

Aster, R.C. & Rowe, C.A., 2000. Advances in seismic event location, in *Automatic Phase Pick Refinement and Similar Event Association in Large Seismic Datasets,* pp. 231–263, eds Thurber, C.H. & Rabinowitz, N., Kluwer Academic Publishing, Amsterdam.

Baer, M. & Kradolfer, U., 1987. An automatic phase picker for local and teleseismic events, *Bull. seism. Soc. Am.,* **77,** 1437–1445.

Bai, C.Y. & Kennett, B.L.N., 2000. Automatic phase-detection and identification by full use of a single three-component broadband seismogram, *Bull. seism. Soc. Am.,* **90,** 187–198.

Bormann, P., Klinge, K. & Wendt, S., 2002. Data analysis and seismogram interpretation, in *IASPEI New Manual of Seismological Observatory Practice (NMSOP),*Vol. 1, Chap. 11, p. 100, ed. Bormann, P., GeoForschungsZentrum, Potsdam, ISBN 3-9808780-0-7.

Di Stefano, R., Aldersons, F., Kissling, E., Baccheschi, P., Chiarabba, C. & Giardini, D., 2006. Automatic seismic phase picking and consistent observation error assessment: Application to the Italian seismicity, *Geophys. J. Int.,* **165,** 121–134.

Douglas, A., Bowers, D. & Young, J.B., 1997. On the onset of P seismograms, *Geophys. J. Int.,* **129,** 681–690.

Earle, P. & Shearer, P.M., 1994. Characterization of global seismograms using an automatic-picking algorithm, *Bull. seism. Soc. Am.,* **84,** 366–376.

Eberhart-Phillips, D. & Michael, A.J., 1993. Three-dimensional velocity structure, seismicity, and fault structure in the Parkfield region, central California, *J. geophys. Res.,* **98,** 737–758.

Fisher, R.A., 1936. The use of multiple measurements in taxonomic problems, *Ann. Eugenics,* **7,** 179–188.

Fisher, R.A., 1938. The statistical utilization of multiple measurements, *Ann. Eugenics,* **8,** 376–386.

Grand, S.P., 1990. A possible station bias in travel time measurements reported to ISC, *Geophys. Res. Lett.,* **17,** 17–20.

Haslinger, F. & Kissling, E., 2001. Investigating effects of 3-D ray tracing methods in local earthquake tomography, *Phys. Earth planet. Inter.,* **123,** 103–114.

Husen, S. & Kissling, E., 2001. Local earthquake tomography between rays and waves: fat ray tomography, *Phys. Earth planet. Inter.,* **123,** 127–147.

Husen, S., Kissling, E., Deichmann, N., Wiemer, S., Giardini, D. & Baer, M., 2003. Probabelistic earthquake location in complex three-dimensional velocity models: application to Switzerland, *J. geophys. Res.,* **108,** 2077.

Kissling, E., 1988. Geotomography with local earthquake data, *Rev. Geophys.,* **26,** 659–698.

Kissling, E., Ellsworth, W.L., Eberhart-Phillips, D. & Kradolfer, U., 1994. Initial reference models in local earthquake tomography, *J. geophys. Res.,* **99**(B10), 19 635–19 646.

Kissling, E., Husen, S. & Haslinger, F., 2001. Model parametrization in seismic tomography: a choice of consequence for the solution quality, *Phys. Earth planet. Inter.,* **123,** 89–101.

Kulhánek, O., 1990. *Anatomy of Seismograms,* Developments in Solid Earth Geophysics 18, Elsevier, Amsterdam.

Kulhánek, O., 2002. The structure and interpretation of seismograms, in *International Handbook of Earthquake and Engineering Seismology. Part A,* pp. 333–348, eds Lee, W.H.K., Kanamori, H., Jennings, P.C. & Kisslinger, C., Academic Press, London.

Leonard, M., 2000. Comparison of manual and automatic onset time picking, *Bull. seism. Soc. Am.,* **90,** 1384–1390.

Leonard, M. & Kennett, B.L.N., 1999. Multi-component autoregressive techniques for the analysis of seismograms, *Phys. Earth planet. Inter.,* **113,** 247–263.

Lippitsch, R., Kissling, E. & Ansorge, J., 2003. Upper mantle structure beneath the Alpine orogen from high-resolution teleseismic tomography, *J. geophys. Res.,* **108**(B8), 2376.

Lombardi, D., Braunmiller, J., Kissling, E. & Giardini, D., 2008. Moho depth and Poisson's ratio in the western-central Alps from receiver functions, *Geophys. J. Int.,* **173,** 249–264.

Podvin, P. & Lecomte, I., 1991. Finite difference computation of travel times in very contrasted velocity models: a massively parallel approach and its associated tools, *Geophys. J. Int.,* **105,** 271–284.

Röhm, A.H.E., Bijwaard, H., Spakman, W. & Trampert, J., 2000. Effects of arrival time errors on traveltime tomography, *Geophys. J. Int.,* **142,** 270–276.

Rowe, C.A., Aster, R.C., Borchers, B. & Young, C.J., 2002. An automatic, adaptive algorithm for refining phase picks in large seismic data sets, *Bull. seism. Soc. Am.,* **92,** 1660–1674.

Rowe, C.A., Thurber, C.H. & White, R.A., 2004. Dome growth behavior at Soufriere Hills Volcano, Montserrat, revealed by relocation of volcanic event swarms, 1995–1996, *J. Volc. Geotherm. Res.,* **134,** 199–221.

Satriano, C., Zollo, A. & Rowe, C.A., 2008. Iterative tomographic analysis based on automatic refined picking, *Geophys. Prospect.,* **56,** 467–475.

Scherbaum, F., 2001. *Of poles and zeros; Fundamentals of Digital Seismology,* Modern Approaches in Geophysics, 2nd edn, Kluwer Academic Publisher, Dordrecht.

Scherbaum, F., 2002. Analysis of digital earthquake signals, in *International Handbook of Earthquake and Engineering Seismology. Part A,* pp. 349–355, eds Lee, W.H.K., Kanamori, H., Jennings, P.C. & Kisslinger, C., Academic Press, London.

Seidl, D. & Stammler, W., 1984. Restoration of broad-band seismograms (Part I), *J. Geophys.,* **54,** 114–122.

Simon, R.B., 1981. *Earthquake Interpretations: A Manual of Reading Seismograms,* William Kaufmann Inc., Los Alto, Ca.

Sleeman, R. & van Eck, T., 1999. Robust automatic P-phase picking: an online implementation in the analysis of broadband seismogram recordings, *Phys. Earth planet. Inter.,* **113,** 265–275.

Solarino, S., Kissling, E., Sellami, S., Smriglio, G., Thouvenot, F., Granet, M., Bonjer, K.-P. & Sleijko, D., 1997. Compilation of a recent seismicity data base of the greater Alpine region from several seismological networks and preliminary 3D tomographic results, *Ann. di Geofis.,* **XL,** 161–174.

Spakman, W., van der Lee, S. & van der Hilst, R., 1993. traveltime tomography of the European-Mediterranean mantle down to 1400 km, *Phys. Earth planet. Inter.,* **79,** 3–74.

Stammler, K., 1993. SeismicHandler - programmable multichannel data handler for interactive and automatic processing of seismological analysis, *Comp. Geosci.,* **19,** 135–140.

Takanami, T. & Kitagawa, G., 1988. A new efficient procedure for the estimation of onset times of seismic waves, *J. Phys. Earth,* **36,** 267–290.

Thurber, C.H., 1983. Earthquake locations and three-dimensional crustal structure in the Coyote Lake area, central California, *J. geophys. Res.,* **88,** 8226–8236.

Um, J. & Thurber, C.H., 1987. A fast algorithm for two-point seismic ray tracing, *Bull. seism. Soc. Am.,* **77,** 972–986.

Virieux, J., Farra, V. & Madariaga, R., 1988. Ray tracing for earthquake location in laterally heterogeneous media, *J. geophys. Res.,* **93,** 6585–6599.

Waldhauser, F., Kissling, E., Ansorge, J. & Mueller, S., 1998. Three-dimensional interface modelling with two-dimensional seismic data: the Alpine crust-mantle boundary, *Geophys. J. Int.,* **135,** 264–278.

Wessel, P. & Smith, W.H.F., 1995. New version of the Generic Mapping Tool released, *EOS, Trans. Am. geophys. Un.,* **76,** 329.

Withers, M., Aster, R., Young, C., Beiriger, J., Harris, M., Moore, S. & Trujillo, J., 1998. A comparison of select trigger algorithms for automated global seismic phase and event detection, *Bull. seism. Soc. Am.,* **88,** 95–106.

Zhang, H., Thurber, C.H. & Rowe, C.A., 2003. Automatic P-wave arrival detection and picking with multiscale wavelet analysis for single-component recordings, *Bull. seism. Soc. Am.,* **93,** 1904–1912.

APPENDIX A: SETS OF FISHER COEFFICIENTS FOR GREATER ALPINE REGION

Table A1. Set of Fishers linear discriminant coefficients for nine predictors and one constant derived from a subset of reference events with $M_l \geq 4.0$. For a detailed description of predictors see Di Stefano *et al.* (2006).

	Automatically assigned quality classes				
Predictors	Class 0	Class 1	Class 2	Class 3	Class 4
Constant	−17.512	−15.671	−15.063	−15.613	−17.041
WfStoN	0.297	0.311	0.302	0.302	0.290
GdStoN	−0.555	−0.360	−0.367	−0.407	−0.407
GdAmpR	0.676	0.429	0.438	0.480	0.473
GdSigFR	0.251	0.233	0.199	0.164	0.152
GdDelF	−0.002	−0.003	0.015	0.026	0.031
ThrCFRat	−0.084	−0.200	−0.212	−0.144	−0.079
PcAboThr	−2.326	−2.416	−2.454	−2.338	−0.493
PcBelThr	0.040	0.051	0.061	0.074	0.100
CFNoiDev	6.141	6.937	7.519	8.128	8.288

Table A2. Set of Fishers linear discriminant coefficients for 9 predictors and one constant derived from a subset of reference picks at epicentral distances $\Delta < 100$ km (predominantly *Pg* phases). For a detailed description of predictors see Di Stefano *et al.* (2006).

	Automatically assigned quality classes				
Predictors	Class 0	Class 1	Class 2	Class 3	Class 4
Constant	−12.940	−11.605	−11.926	−13.219	−26.743
WfStoN	0.205	0.201	0.210	0.254	0.242
GdStoN	−0.357	−0.246	−0.198	−0.395	−0.644
GdAmpR	0.272	0.117	0.086	0.280	0.547
GdSigFR	0.260	0.276	0.215	0.218	0.182
GdDelF	−0.053	−0.033	−0.010	−0.023	−0.023
ThrCFRat	0.128	−0.015	0.026	−0.028	−0.003
PcAboThr	−1.582	−1.748	−1.253	−0.838	6.376
PcBelThr	0.044	0.069	0.143	0.096	0.159
CFNoiDev	3.591	4.445	4.544	4.787	5.387